

The limitations of hydrodynamic removal of biofilms from the dead-ends in a model drinking water distribution system

Urh Simunič¹, Peter Pipp², Matevž Dular², David Stopar^{1*}

¹University of Ljubljana, Biotechnical Faculty, Jamnikarjeva 101, 1000 Ljubljana, SI-Slovenia

²University of Ljubljana, Faculty of Mechanical Engineering, Aškerčeva 6, 1000 Ljubljana, SI-Slovenia

* Correspondence to: Prof. dr. David Stopar, University of Ljubljana, Biotechnical Faculty, Jamnikarjeva 101, 1000 Ljubljana, SI-Slovenia, email: david.stopar@bf.uni-lj.si

ABSTRACT

Biofilm formation and removal from dead-ends is a particularly difficult and understudied area of water distribution system biology. In this work, we have built a model drinking water distribution system to probe the effect of different hydrodynamic flow regimes on biofilm formation and removal in the main pipe and in the dead-end. The test rig was built to include all major drinking water distribution system components with materials and dimensions used in the standard plumbing system. We have simulated the effect of stagnant, laminar, turbulent, and intense turbulent flushing conditions on the growth and removal of biofilms from the main pipe and the dead-end. The growth of the biofilm in the main pipe was not prevented at a volumetric flow rate of $9.4 \text{ L} \cdot \text{min}^{-1}$ and flow velocity of $2 \text{ m} \cdot \text{s}^{-1}$. Mature biofilms were more difficult to remove. Biofilms grown under shear stress conditions could withstand significantly higher shear stresses than those to which they were exposed to during the growth. The biofilms grew twice as fast in the dead-end when flow in the main pipe was turbulent compared to stagnant conditions. Biofilms in the dead-end were not affected by the flushing conditions in the main pipe ($Q = 52 \text{ L} \cdot \text{min}^{-1}$, $Re = 9.0 \cdot 10^4$). The computational fluid dynamics simulation suggests that biofilms cannot be hydrodynamically removed from the dead-end at depths that are larger than one pipe diameter. Biofilms beyond this limit present a possible source for reinoculation and recolonization of the rest of the water distribution system.

Keywords: biofilm control, drinking water distribution systems, hydrodynamic flow, dead-ends, *Escherichia coli*

INTRODUCTION

A biofilm is a self-made composite of organic and inorganic material produced by microorganisms on different surfaces in contact with water. A biofilm is a diverse microbial community that includes bacteria, viruses, fungi, and protozoa. Biofilms in drinking water distribution systems (DWDS) can cause a wide range of water quality and operational problems (Liu et al., 2016). They can be responsible for increased bacterial levels in the distribution system, reduction of dissolved oxygen, loss of distribution system disinfectant residuals, taste and odour changes, water coloration (i.e. red or black color due to iron or sulfate-reducing bacteria), microbial-induced pipe corrosion, hydraulic roughness, and reduced materials life (Characklis and Marshal, 1990).

The primary reason that many water utilities are concerned with biofilms in DWDS is due to growth of coliform bacteria in the pipe network that violate drinking water standards. The occurrence of coliform bacteria in DWDS is influenced by water filtration, temperature, disinfectant type, source of organic carbon level, corrosion control, pipe material selection, faulty parts of the system or other operational defects (Liu et al., 2016; Simões L. C. and Simões M., 2013). A majority of the DWDS that are affected by coliform bacteria can trace their problems to the growth of biofilms (LeChevallier, 2003). Due to the protection offered by the microbial self-produced extracellular polymeric matrix, biofilms are difficult to control and practically impossible to eliminate. The extracellular matrix protects microorganisms within biofilms from a variety of external adverse factors including fluid flow and chemical disinfection (Douterelo et al., 2016).

High flow velocities may result in self-cleaning and are regularly applied in DWDS to ensure the removal of sediment and biofilms. The effect of fluid-flow velocity on microbial growth and biofilm formation has been studied in a pilot-scale water hydraulic system (Soini et al., 2002). Microbes attached to surfaces both under low and high shear stresses. During flushing, the shear stress is transiently raised to even higher values to mobilize particulate material and bacteria from the pipe walls into the bulk flow. Although this prevents short-term water quality issues, it is generally not capable of eliminating all the biofilm, and bacteria can regrow (Douterelo et al., 2013).

Far more problematic than biofilms grown in the main pipe system are biofilms that grow in zones of water stagnation or in parts of the system known as dead-ends with long water residence times (Liu et al., 2019; Smith et al., 1999; Barbeau et al., 2005; Ling et al., 2018). It is generally accepted that water in dead-end pipes is not circulated (Liu et al., 2006; Smith et al., 1999; Zlatanović et al., 2017). Dead-ends are associated with high organic material sedimentation, favourable corrosion conditions, absence of residual disinfectants and pose a high risk to health (Barbeau et al., 2005; Carter et al., 1997). Studies of water distribution systems have shown that bacteriological hot spots are three to four times more likely to occur at dead-ends (Elgamal and Farouk, 2019). In purging saline solution from a dead-end pipe it was shown that as the distance of purging location from the dead-end increased, the removal time increases exponentially. This suggests that the removal of biofilms from dead-end zones in DWDS is likely to be ineffective. There are, however, very few reports on the rate of growth and removal of biofilm from dead-ends in real drinking water distribution systems.

The aim of the research reported here is to determine biofilm growth, removal, and mobilization patterns in the dead-end zone of a model DWDS under different flow regimes in the main pipe. The *E. coli* biofilms were either grown in the model DWDS or were grown exogenously in the

lab and introduced to the model DWDS. The test rig was built to include all the major DWDS components (i.e. water storage tank, valves, pump, measuring cell, main flow, and dead-end zones) with materials and dimensions used in the standard plumbing system. In the model DWDS, we have simulated stagnant, laminar, turbulent, and intense turbulent flushing conditions. The biofilm surface coverage in the main pipe and in the dead-end zone was determined at different flow regimes in the main pipe.

Materials and methods

1. Model drinking water distribution systems (DWDS)

The customarily built test rig is shown in Fig. 1A. It was constructed of polyvinyl chloride pipes (13 mm diameter), submersible pump Maxijet 1000 aquarium pump (Aquarium Systems, France), with $Q_{\max} = 16.7 \text{ L} \cdot \text{min}^{-1}$ controlled by a variable autotransformer HSN0303 (Metrel, Slovenia), or a more powerful pump GP 4500 INOX (TIP Technische Industrie Produkte GmbH, Germany) with a working volume of 1600 mL and Q_{\max} of $72.5 \text{ L} \cdot \text{min}^{-1}$ controlled by OPTIDRIVE E2 (Invertek Drives, United Kingdom), Processmaster 610 (ABB GmbH, Germany) flow meter, and the customary made measuring flow cell that allowed growth of the biofilm in the DWDS or enabled insertion of the exogenously grown biofilm in the test rig. The working volume of the system was 600 or 2200 mL in the case of the more powerful pump. The system allowed regulation of the flow in the Re range from $1 \cdot 10^3$ to $9 \cdot 10^4$. Biofilms were either grown on the microscopic slides in the flow cell or exogenously in the microbiological lab and later inserted in the flow cell. After the experiment, the microscopic slides were removed from the flow cell and microscopically analysed. To check the effect of the dead-end zone on the growth and removal of the biofilm the test rig was modified as given in Fig. 1B.

Perpendicular to the main pipe system the dead-end pipe was attached via a T junction. The length of the dead-end pipe was 56 mm. At the end of the dead-end pipe, a measuring flow cell closed at the distal end was attached.

To clean it the model water distribution system was disassembled and the inside of the system was mechanically scrubbed with a commercial detergent solution. The excess detergent was rinsed with tap water. The system was assembled and disinfected with 70 % (v/v) ethanol and rinsed again with tap water. Since only green fluorescent protein-expressing *E. coli* were used in the experiments, the background bacterial contaminations introduced with tap water were not visible in our experiments because they were not capable of growing on the selective growth medium supplemented with kanamycin.

To study the effect of flow regimes on the growth and removal of bacterial biofilms, a stainless steel flow cell was built to allow the insertion of the poly(methyl methacrylate) (PMMA) slides with biofilms. The flow cell is shown in Fig. 1C,D. It is composed of the body of the flow cell with a rectangular flow profile and a removable lid. The dimensions of the flow channel were $266 \times 10 \times 10$ mm. The PMMA slides were attached to the flow cell with a rubber fitting.

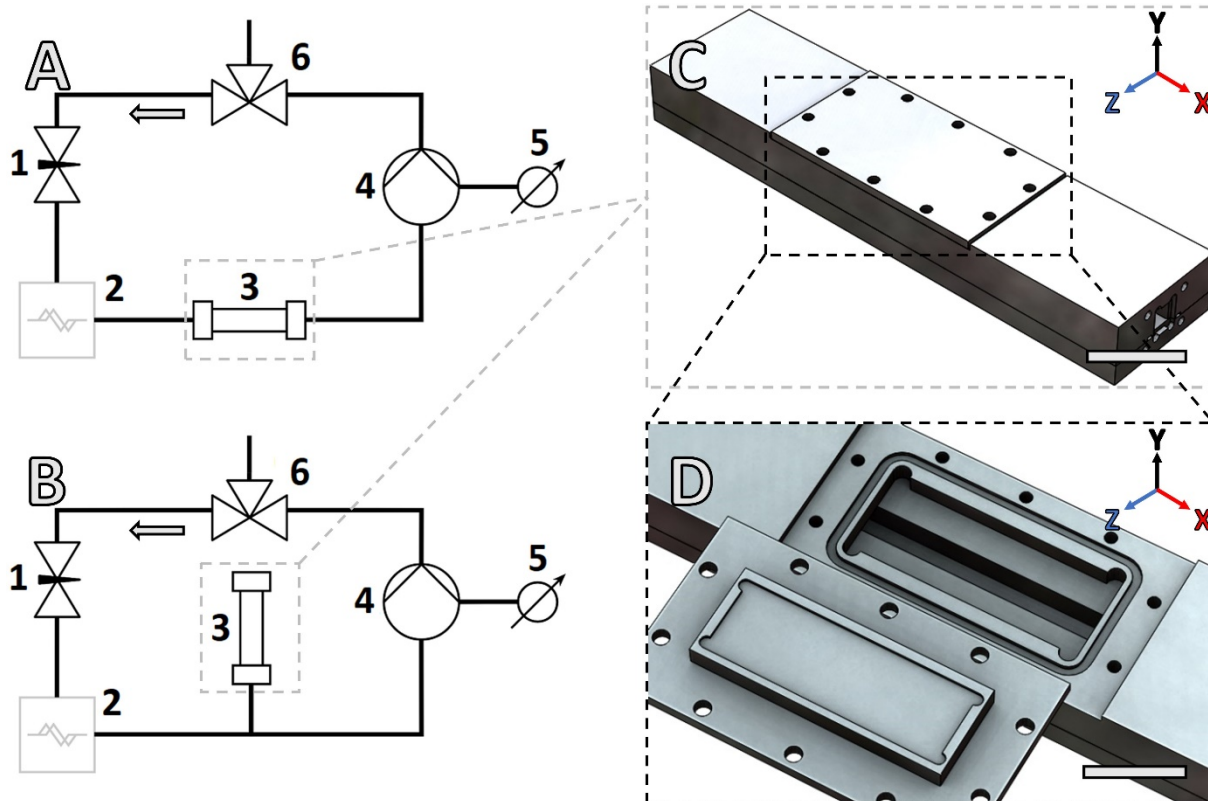


Figure 1: Schematic illustration of the model DWDS used to determine the effect of flow regimes on growth and removal of *E. coli* biofilms. (A) Model DWDS with the flow cell connected to the main pipe. (B) Model water distribution system with the flow cell connected to the dead-end pipe. Inset: (C) Assembled flow cell, scale bar = 5 cm. (D) Disassembled flow cell with the lumen of the square duct exposed, scale bar = 3 cm. The flow direction in A and B is indicated with an arrow, in C and D it is along the X-axis. Model water distribution system components: reducing valve (1), flow meter (2), flow cell (3), aquarium or submersible pump (4), variable autotransformer (when using aquarium pump) or frequency drive (when using submersible pump) (5), three-way ball valve (6). During biofilm growth and removal experiments, the flow meter was not connected to the model DWDS.

Prior to the insertion, the adhesive tapes on the PMMA slides, that limited bacterial lateral growth, were removed. Next, the slide was inserted into the flow cell and the lid was screwed into the flow cell. The assembled model DWDS was filled with tap water and excess air vented

through the valve. After insertion of the slides with biofilms into the flow cell, the biofilm was incubated for 10 minutes under stagnant conditions. The samples were subjected to different flow regimes as given in Table 1. The Reynolds number was calculated as:

$$Re = \frac{u_{avg} \cdot d}{\nu} \quad \dots(1)$$

where the pipe diameter d is used for the length scale and the average cross-sectional velocity u_{avg} , ν is kinematic viscosity. In the case of a rectangular channel, the hydraulic diameter was determined as:

$$d = \frac{4 \cdot A}{C} \quad \dots(2)$$

where A is the cross-section area and C is the circumference (Elger et al., 2012).

Table 1: Flow regimes used in this study. Flow velocity and Reynolds number were derived from volumetric flow rates. The transition from laminar to turbulent flow in a pipe usually occurs at Re between 2000 and 2500 in the case of circular and rectangular cross-sections (Tosun et al., 1988). In this paper, $Re = 2200$ was denoted as a transitional state.

Flow regime (corresponding number)	Volumetric flow rate Q [L · min ⁻¹]	Flow velocity u_{avg} [m · s ⁻¹]	Reynolds number Re	Average shear stress τ_{wall} [Pa]	Pump used
Stagnant conditions(0)	0	0	0	0	aquarium or submersible pump
Laminar flow regime (1)	0.6	0.10	1000	0.07	aquarium pump
Transitional flow regime (2)	1.3	0.20	2200	0.32	aquarium pump

Turbulent flow regime (3)	9.4	1.60	16000	7.53	aquarium pump
Turbulent flow regime (4)	8.8	1.47	15000	6.71	submersible pump
Turbulent flow regime (5)	17.6	2.93	30000	22.71	submersible pump
Turbulent flow regime (6)	26.3	4.38	45000	46.82	submersible pump
Turbulent flow regime (7)	35.6	5.93	60000	80.24	submersible pump
Turbulent flow regime (8)	52.0	8.67	90000	158.84	submersible pump

2. Growth of *Escherichia coli* biofilms outside the flow system

Escherichia coli MG1655, DE3 designated as *E. coli* was used in all experiments. The strain carries a plasmid with resistance to kanamycin and contains a gene for constitutive expression of a green fluorescent protein (gfp) (Horvat et al., 2019; Lorenzetti et al., 2015). Bacteria were grown on Lysogeny Broth (LB-Km) agar (1 % (w/v) tryptone, 0.5 % (w/v) yeast extract, 0.5% (w/v) NaCl, and 1.5 % (w/v) agar), supplemented with kanamycin sulfate ($50 \mu\text{g} \cdot \text{mL}^{-1}$). A single *E. coli* colony was aseptically transferred from the Petri dish to 10 mL of liquid LB medium (without kanamycin). The inoculated medium was incubated overnight at 37 °C, 200 rpm. Next, 700 μL of the overnight culture was diluted to an optical density OD_{650} of 0.05 (a.u.) and transferred to a pre-sterilized PMMA slide (6 % (v/v) hydrogen peroxide for 15 minutes, rinsed twice with PBS) placed in a sterile Petri dish. The left and right sides of the PMMA slides (75 mm \times 25 mm \times 2 mm Acrytech, Slovenia) were covered with adhesive tape to prevent lateral biofilm growth. To grow immature biofilms the inoculated slides were pre-incubated for two hours to allow the bacterial cells to adhere to the surface. The slides were then transferred

into a sterile 50 mL centrifuge tube with a conical bottom to which 30 mL of liquid LB medium with 2.2 % (w/v) lactose was added (Baš et al., 2017). The tubes were sealed and incubated horizontally at 37 °C without shaking. Every 24 hours, the spent medium was aseptically drained and the same volume of liquid LB medium with lactose was replaced. After 72 hours of incubation, the spent culture medium was discarded and the weakly adhered cells were removed from the slide by immersing the slides in 50 mL of PBS. The submerged slides were shaken gently in a circular motion for about 10 seconds, turned to the side and carefully removed from the buffer. Excess fluid on the slides was removed by pressing the edge of the glass for a few seconds against a paper towel. The process was repeated three times. The control sample slides were prepared only with medium to check for contaminations. The washed biofilm slides were kept in a sealed centrifuge to prevent desiccation prior to the transfer into the measuring flow cell. To grow mature biofilms, pre-sterilized PMMA slides were incubated with 500 µL of overnight *E. coli*, suspended in 21.5 mL of liquid LB medium with 2.2 % (w/v) lactose. This time PMMA slides were incubated horizontally rotated by 90° along the slide's long axis so that a thick biofilm formed at the air-liquid interface. The spent growth media was replaced every 24 h of incubation. With each replacement, 1 mL of extra growth media was added, which allowed for an extra band of thick biofilm to grow at the air-liquid interface. Different bands of the biofilm merged at the end of incubation, forming a mature biofilm. The immature or mature biofilms were aseptically transferred to the flow cell. Biofilms that were grown outside the flow cell were hydrodynamically treated at room temperature.

3. Growth of Escherichia coli biofilms in the flow cell

Before each experiment, the model DWDS was disassembled and the flow cell was mechanically cleaned by scrubbing using a commercial detergent solution and rinsed with tap water. The assembled model water distribution system was then chemically sterilized with 6 %

(v/v) hydrogen peroxide for at least 30 minutes at room temperature. Periodically turbulent conditions were established for a shorter time ($Q = 9.4 \text{ L} \cdot \text{min}^{-1}$, $t = 1 \text{ min}$). The hydrogen peroxide was drained and DWDS rinsed with sterile deionized water. The ball valve was sterilized by dipping it in 70 % (v/v) ethanol, which was then burned off. To maintain 37 °C during the growth of the biofilm the model DWDS was placed into a microbiological incubator room at 37 °C. All tests were performed in two independent experiments. The data for surface coverage were determined at 16 different positions, for CFU three replicates were done. The DWDS was filled with sterile LB medium with 2.2 % (w/v) lactose and inoculated with an overnight culture of *E. coli* to the final concentration of $1 \times 10^6 \text{ CFU} \cdot \text{mL}^{-1}$. The biofilms were grown at 37 °C for 48 hours under stagnant conditions or turbulent flow regime (flow regimes 0 or 3 in Table 1, respectively). After every 24 hours, the spent medium was replaced with fresh medium. The spent culture medium was drained, the ball valve re-sterilized, and the system filled with the fresh LB medium with added lactose. The flow cell was inserted either in the main pipe system (Fig. 1A) or in the dead-end (Fig. 1B). Biofilms grown under stagnant conditions or turbulent flow regime were subjected to flow regimes 0 and 8 as described in Table 1. Biofilms that were grown in the flow cell at 37 °C were, for technical reasons, hydrodynamically treated at 20 °C.

4. Microscopy of biofilms

Biofilms were sampled by stopping the flow, removing the lid of the flow cell and removing the PMMA slide with biofilm. The slides were washed three times in sterile PBS to remove weakly adhered cells. Axio Observer Z1 inverted microscope (Zeiss, Germany) was used to observe the biofilms with differential interference contrast technique (DIC) and fluorescence. Microscopy was performed at 20x magnification (20x/0.4 lens). At the end of microscopy,

PMMA slides were stained with crystal violet dye solution to determine the biofilm surface coverage.

5. Biofilm surface coverage

The slides with biofilms were air-dried and flame fixed. The fixed biofilms were stained by 1 % (v/v) crystal violet solution (Merck, Germany) for 10 minutes, washed and air-dried. The slides were analyzed with a DM300 light microscope (Leica Microsystems, Germany) or Axio Observer Z1 inverted microscope (Zeiss, Germany). Images were captured at 400x magnification every 5 mm along the centerline of the slide, from the inlet to the outlet side of the flow cell, in total 16 images on each slide. The individual images for each slide were analyzed with Fiji (version 1.52c) to obtain the biofilm surface coverage using a triangle method and an ImageJ measuring function (Zack et al., 1977). The images were converted to binary format with a black background and white biofilm, with an automatically determined threshold value that separates the biofilm from the background. Visual noise was removed from all the images in the set, using the “despeckle” function. The average surface coverage A [%] of individual slides was then calculated using Equation 3:

$$A = \frac{\sum A_x}{n} \quad \dots(3)$$

where A_x is the percentage of the surface of the PMMA slide covered with biofilm at a certain distance x [mm] from the inlet side of the PMMA slide and n is the number of microscopic measuring sites.

6. Concentration of planktonic bacteria in the model DWDS

Planktonic bacteria in the model DWDS were sampled via the ball valve. Approximately 50 mL of liquid was sampled during the model DWDS operation to obtain a representative microbiological sample. 10-fold serial dilutions were prepared from the sampled water. Next, 20 μL of serial dilutions were applied to the LB-Km agar plates using the plate drop method. The plates were pre-incubated at room temperature until no liquid was observed and then incubated at 28 °C for 16 hours. The plates with the number of colonies between 2 and 20 colonies were counted (Herigstad et al., 2001). The control of cleaning was performed in three replicates on PCA agar plates (0.5 % (w/v) tryptone, 0.25 % (w/v) yeast extract, 0.1 % (w/v) glucose and 0.9 % (w/v) agar; calibrated to pH value of 7.0). No growth was observed in the control samples.

7. Hydrodynamic flow simulation

Computational fluid dynamics simulation as described by Teodósio et al., 2012 and Teodósio et al., 2013 has been applied using ANSYS R19.2 software to construct the flow cell and the relevant regions of the model water distribution system. Based on the geometry of the model DWDS, we created a computational grid with hexahedral elements. The basic size of each control volume was 1 mm, while the size of the control volumes in the observation area was 0.5 mm. Three mesh sizes were tested in the main pipe and in the dead-end simulations. The mesh sizes are given in Table 2.

Table 2: Mesh size selection (the number of control volumes) for the hydrodynamic flow simulation in the main pipe and in the dead-end.

Mesh	Size (main pipe)	Size (dead-end)
------	------------------	-----------------

Coarse	69676	90617
Medium	213300	255833
Fine	937938	922721

Velocity profiles at a position were compared and Richardson extrapolation (Ferziger and Perić, 2002) was used to evaluate the mesh dependence. In all, local flow velocities at 700 points were compared. It was concluded that by using the mid-size grid, the error was approximately 3 %, which was acceptable for the purpose of the present study. The computational domain in the main pipe consisted of 213300 elements, while in the case of the dead-end, the computational grid consisted of 255800 elements. In both cases, we resorted to the use of symmetry, so that only half of the total geometry of the model distribution systems were calculated. The fluid parameters were: density $998.2 \text{ kg} \cdot \text{m}^{-3}$, dynamic viscosity of $1.003 \cdot 10^{-3} \text{ Pa} \cdot \text{s}$ and operating pressure 1013.25 hPa. The hydrodynamic flow simulations were performed at 20 °C. We have also checked the effect of temperature on flow dynamics at 37 °C. The two flow regimes were not statistically different. For the boundary conditions, an appropriate mass flow rate at the inlet and the standard pressure at the outlet were defined. A stationary wall with no-slip condition was assumed. In the case of turbulent flow, a standard roughness model was used (Sommerfeld and Huber, 1999), with a roughness height of 0 m and a roughness constant of 0.5. For lower volumetric flow rates ($Q = 0.6 \text{ L} \cdot \text{min}^{-1}$), laminar flow was assumed. For higher volumetric flow rates ($Q = 9.4 \text{ L} \cdot \text{min}^{-1}$, $35.6 \text{ L} \cdot \text{min}^{-1}$ and $52.0 \text{ L} \cdot \text{min}^{-1}$), turbulent flow was assumed, the solution of which was obtained using the SST $k-\omega$ turbulent model (Menter, 1994). Numerical simulations were performed as steady-state Reynolds-averaged Navier-Stokes equations with a pressure-based SIMPLE algorithm (Patankar, 1980) for the pressure-velocity coupling method. Second-order spatial discretization was used for all equations and absolute residuals were set to $1e-6$, except for the continuity for which they were set to $1e-4$. In addition to the local values of flow velocity within the model DWDS, the model solutions also provided

values for local shear stress. Numerical simulation was done in 3D with a symmetry plane (half of the domain was modeled). The results (contour plots) are only shown in planes in the middle cross-section of the pipe. For graphical presentation, the data for the flow velocity and shear stress were normalized. The values for the flow velocity were normalized using Equation 4:

$$u_{i,\text{norm}} = \frac{u_i}{u_{\text{max}}} \quad \dots(4)$$

where $u_{i,\text{norm}}$ is the normalized value for the flow velocity, u_{max} [$\text{m} \cdot \text{s}^{-1}$] is the maximum value for the flow velocity within the data set, and u_i [$\text{m} \cdot \text{s}^{-1}$] is a specific value for the flow velocity within the data set. The values for the shear stress were normalized using Equation 5:

$$\tau_{i,\text{norm}} = \frac{\tau_i}{\tau_{\text{max}}} \quad \dots(5)$$

where $\tau_{i,\text{norm}}$ is the normalized value for the shear stress, τ_{max} [Pa] is the maximum value for the shear stress within the data set, and τ_i [Pa] is a specific value for the shear stress within the data set.

8. Statistical data analysis

Statistics were performed in OriginPro 2016. One-way analysis of variance ANOVA was used at a significance level of $\alpha = 0.05$. A *post hoc* Tukey test was subsequently performed to discriminate between the sample pairs. To check for a significant difference between the initial and final states of the samples, we used Student's t-test at a significance level of $\alpha = 0.05$. We used the Pearson correlation coefficient to determine the correlation between the data. A normal distribution was assumed for all the data. A logistic function was used to fit the data of biofilm surface coverage and the concentration of planktonic bacteria.

RESULTS

1. Biofilm removal from the main pipe

The effect of different flow regimes (laminar, transitional or turbulent) on the removal of *E. coli* biofilms from the main pipe is shown in Fig. 2. The surface covered with biofilms and the concentration of planktonic bacteria in the model DWDS were dependent on the flow regime. As Reynolds number increased, the biofilm surface coverage decreased significantly ($F(4,10) = 66.92; p < 0.001$), consistently the concentration of planktonic bacteria in the flow circulation increased ($F(4,10) = 7.91; p = 0.004$). As indicated by the positive control sample, the insertion of the biofilm in the flow cell perturbs the biofilm and significantly reduces its surface coverage ($p < 0.001$). These results suggest that there are two populations of cells in the biofilm. A population of weakly adhered (sedimented) bacteria, which can already be removed by inserting the biofilm slide into the flow cell, and a population of strongly adhered cells, which can be partially washed at different flow regimes. To study the effect of hydrodynamic flow on strongly adhered cells, the sedimented bacteria were removed prior to the next experiments.

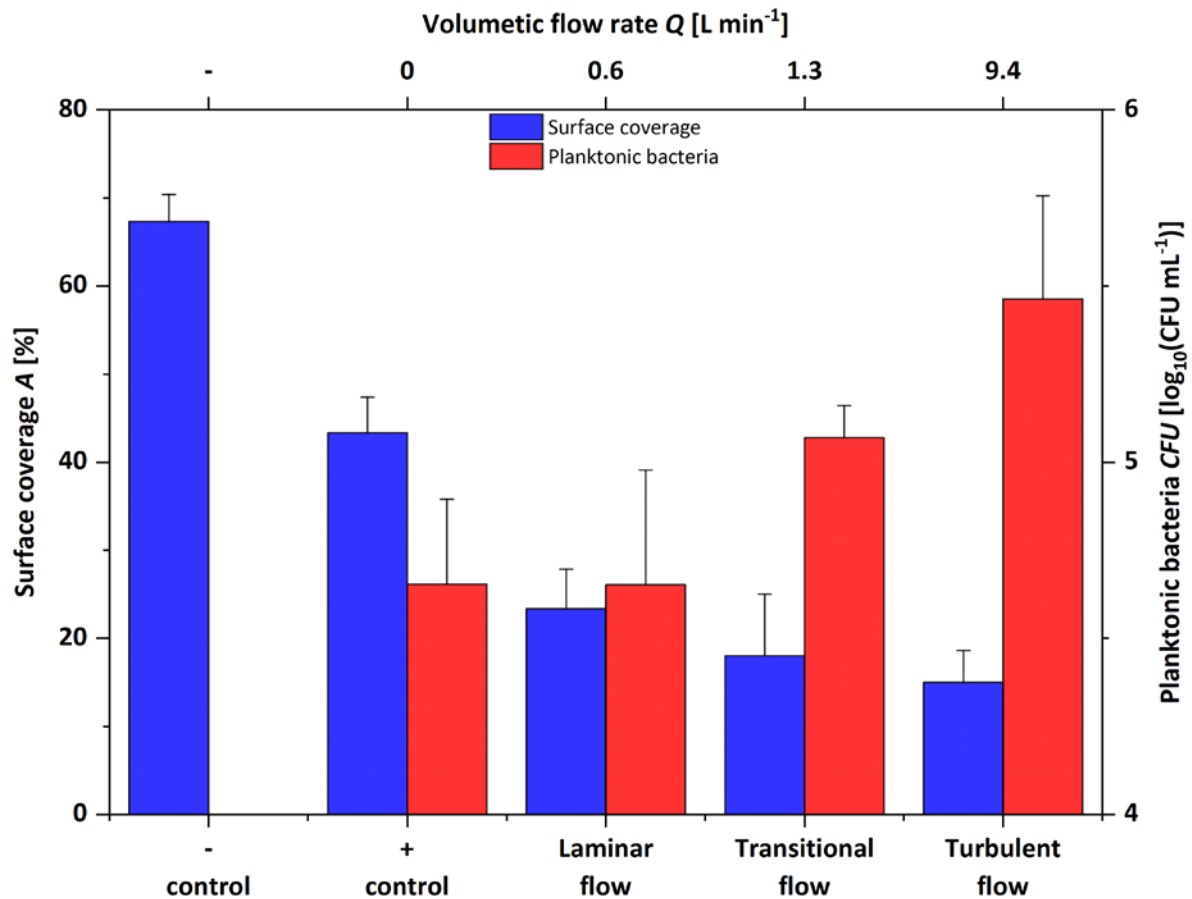


Figure 2: Surface coverage of *E. coli* biofilm and the concentration of planktonic bacteria in the model DWDS depending on the flow regime (positive control: $Re = 0$, $t = 600$ s; laminar: $Re = 1 \cdot 10^3$, $t = 330$ s; transitional: $Re = 2.2 \cdot 10^3$, $t = 150$ s; turbulent flow: $Re = 1.6 \cdot 10^4$, $t = 21$ s). The negative control represents the slide, covered with biofilm which was not inserted into the flow cell. The positive control was the slide with biofilm inserted into the flow cell and incubated for 10 minutes under stagnant conditions and then removed from DWDS. In all flow conditions, the same volume of fluid (3.3 L) was circulated over the biofilm. The mean values \pm SD ($n = 3$) are shown.

Because biofilms were not completely removed from the surface of PMMA slides even after 90 min of exposure to the turbulent flow regime ($Re = 1.6 \cdot 10^4$, $Q = 9.4$ L \cdot min⁻¹), we increased the flow by installing a stronger pump in the model DWDS capable of generating $Q = 52.0$ L \cdot min⁻¹ and $Re = 9.0 \cdot 10^4$. The effects of increased flow rate on the immature and mature biofilm removal are shown in Fig. 3. The biofilm surface coverage and the concentration of planktonic

bacteria in the circulating flow for both the mature and immature biofilm were dependent on the Reynolds number. As Re increased, the surface coverage decreased and the concentration of planktonic bacteria increased ($r = -0.82$; $p < 0.001$ and $r = -0.84$; $p < 0.001$ for the immature and mature biofilm, respectively). We have fitted a logistic curve to the biofilm surface coverage and the concentration of planktonic bacteria data. At Re values $< 1.5 \cdot 10^4$ the removal of cells from the immature biofilm was very small. Above $Re = 1.5 \cdot 10^4$ (EC_{10}) the concentration of planktonic bacteria increased rapidly. Above $Re = 3.8 \cdot 10^4$ (EC_{90}) the concentration of bacteria in the circulating flow no longer increased. Similar observations were made for the mature biofilms. On the other hand, the biofilm surface coverage decreased rapidly above $Re = 1.9 \cdot 10^4$ (EC_{90}) and $5.2 \cdot 10^4$ (EC_{90}) for the immature and mature biofilms, respectively. The biofilm surface coverage did not change much above $Re = 8.1 \cdot 10^4$ (EC_{10}) and $Re = 9.6 \cdot 10^4$ (EC_{10}) for the immature and mature biofilms, respectively. The logistic model suggests that for complete removal of bacterial cells in a mature biofilm, Re in excess of 10^5 should be used, which is unattainable for most drinking water distribution systems.

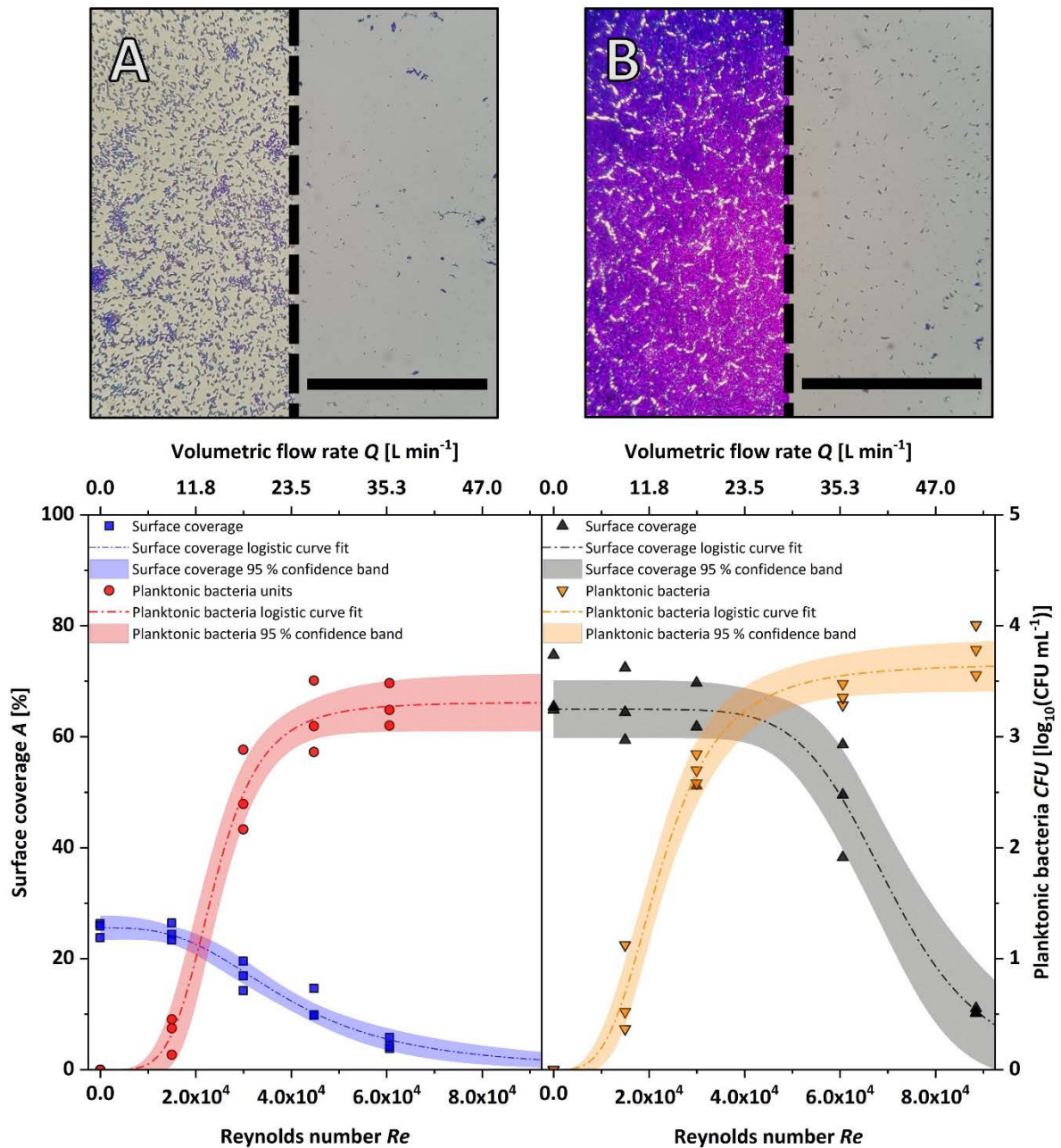


Figure 3: Above; representative images of the immature *E. coli* biofilms (A) and the mature *E. coli* biofilms (B), stained with crystal violet. The dashed line separates the images of biofilms obtained after 10 min of incubation under stagnant conditions and after flushing with Reynolds number $6 \cdot 10^4$ for the immature biofilm or $9 \cdot 10^4$ for the mature biofilm. Scale = 200 μm . Below; the surface coverage and the concentration of planktonic bacteria, depending on the Reynolds number or volumetric flow rate in the main pipe. The primary Y-axis shows surface coverage, the secondary Y-axis shows the concentration of planktonic bacteria in the circulation flow. The flushing time was 1 min in all cases. Data for immature biofilms are shown on the left and for mature biofilms on the right. The values of independent repetitions are shown ($n = 3$).

2. Biofilm removal from the dead-end

The results for the model DWDS with the included dead-end pipe are given in Fig. 4. During the experiment, the volumetric flow rate in the main pipe was $Q = 35.6 \text{ L} \cdot \text{min}^{-1}$ and $Q = 52.0 \text{ L} \cdot \text{min}^{-1}$ for the immature and mature biofilms, respectively. These flow rates were selected because they had the highest biofilm removal rate in the main pipe. In sharp contrast, in the dead-end pipe, neither surface coverage nor the concentration of planktonic bacteria changed significantly with the flow in the main pipe.

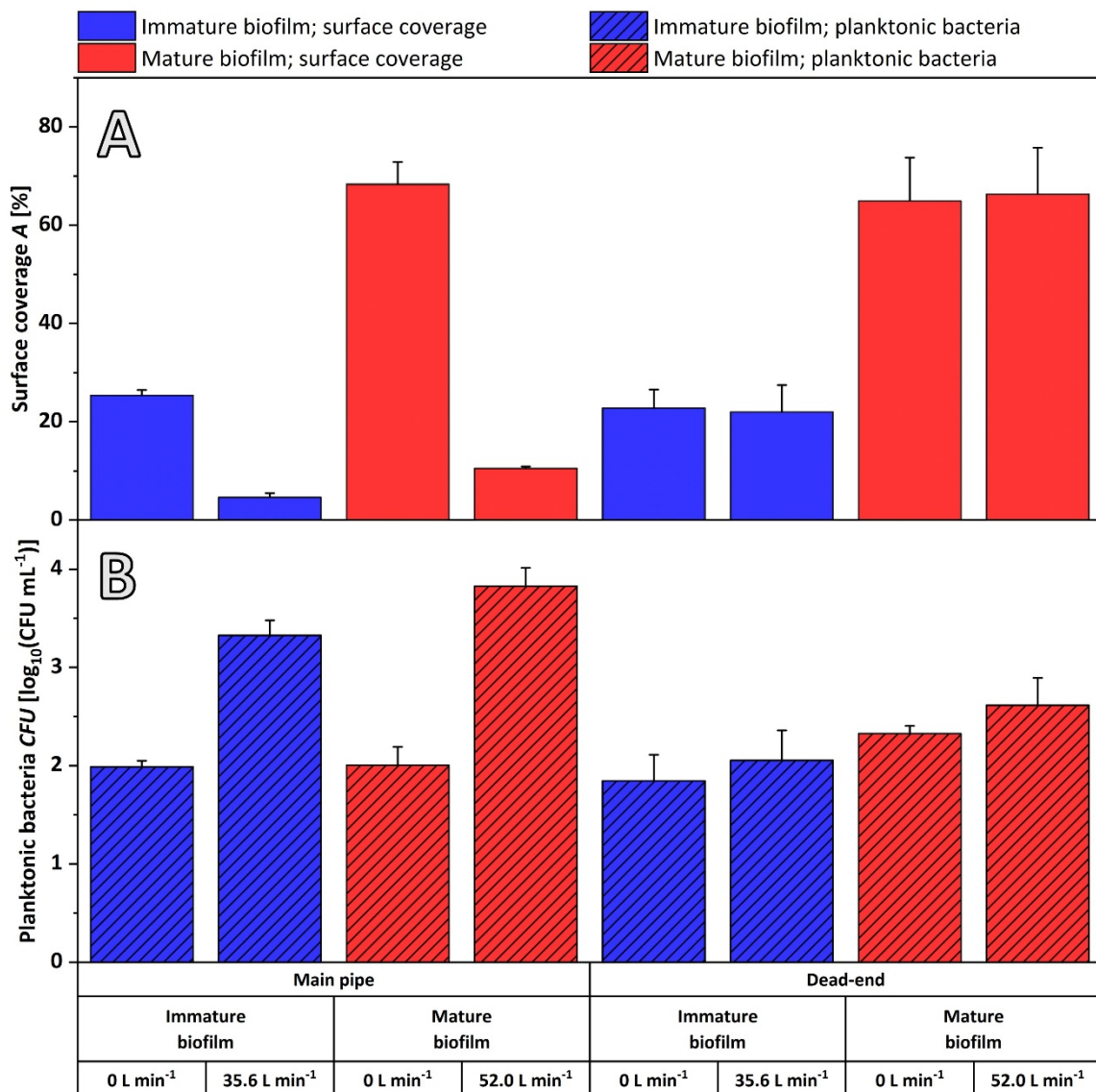


Figure 4: Surface coverage of immature and mature *E. coli* biofilms (A) and the concentration of planktonic bacteria in the model DWDS (B) in the main pipe and in the dead-end depending on the volumetric flow rate of the fluid in the main pipe. The figure also summarizes the results of Figure 3. Mean values \pm SD are shown (n = 3).

3. Removal of biofilm grown in situ in the model DWDS

The results presented so far were for biofilms grown on PMMA slides outside the model DWDS under no shear conditions that were then transferred to the flow cell. To check if the results are similar for the biofilms grown in the distribution system, we have grown biofilms in the model DWDS under no shear or shear conditions. The representative morphologies of the biofilms grown in the model DWDS are shown in Fig. 5. Under no shear conditions in the DWDS, a patchy distribution of multilayer biofilms formed. Whereas under shear conditions in the main pipe, much less biofilm formed. The biofilms were granular and formed small rounded clusters, with an average diameter of $(14 \pm 1) \mu\text{m}$ containing on average (32 ± 11) cells in a single layer. When biofilms grew in the main pipe under shear conditions ($Q = 9.4 \text{ L} \cdot \text{min}^{-1}$) and after growth were subjected to flushing conditions (i.e. $Q = 52.0 \cdot \text{L min}^{-1}$), the surface coverage did not decrease significantly. Biofilms that grew in the dead-end under no-shear conditions had a similar morphology to the biofilms grown in the main pipe. Surprisingly, however, biofilms in the dead-end growing under turbulent flow conditions in the main pipe formed very thick multilayer biofilms. The biofilms in the dead-end were not affected by flushing conditions in the main pipe.

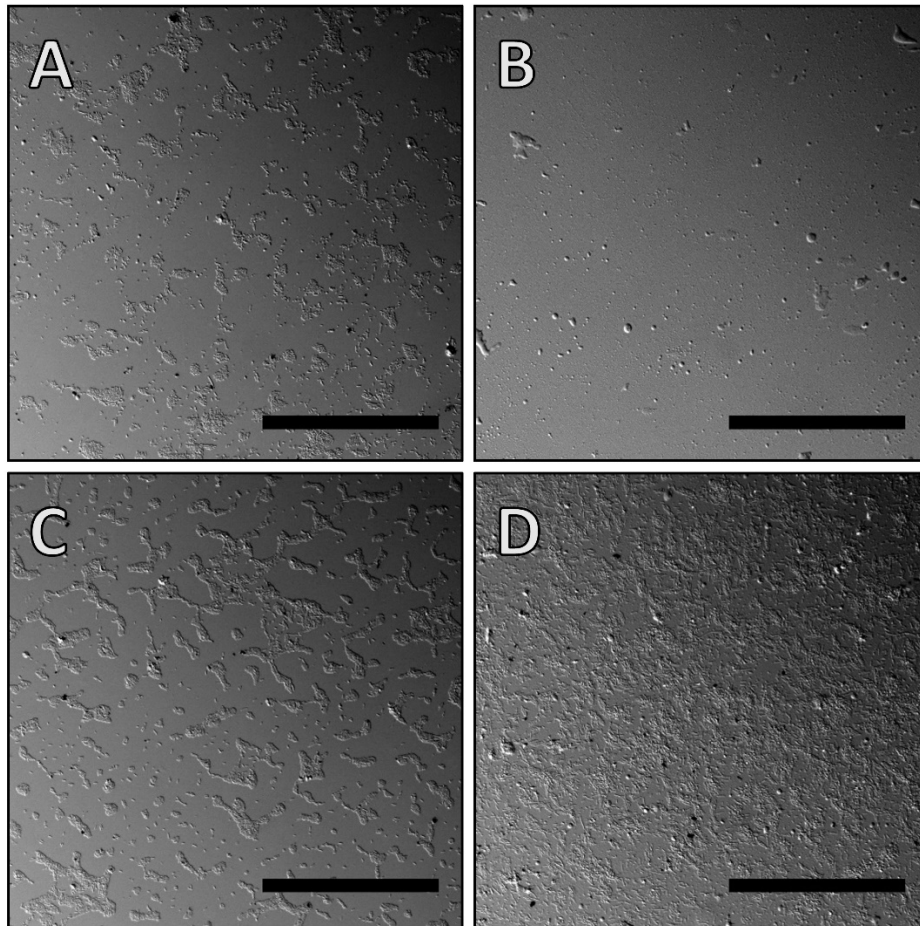


Figure 5: Representative images of biofilms grown on PMMA slides under no shear or shear stress conditions in the model DWDS obtained by DIC microscopy. The top row shows *E. coli* biofilms in the main pipe formed after two days of growth under no shear (**A**) and turbulent ($Re = 1,6 \cdot 10^4$) shear conditions (**B**). The bottom row shows biofilms, formed after two days of growth in the dead-end pipe of the model DWDS under no shear (**C**) and turbulent shear flow regime in the main pipe (**D**). Scale bar = 200 μm .

The biofilm surface coverage in the main pipe and in the dead-end grown under shear or no-shear conditions are given in Fig. 6. In the main pipe, the biofilm surface coverage decreased approximately 6-fold with turbulent flow ($F(3,4) = 97.53$; $p < 0.001$). On the other hand, in the dead-end pipe, the opposite effect was observed. With shear in the main pipe, the surface coverage increased approximately two-fold. Under no-shear conditions, there was no difference

between the main pipe and the dead-end ($p = 0.367$). During the experiment, the concentration of planktonic bacteria increased significantly in all experiments (Fig 6B).

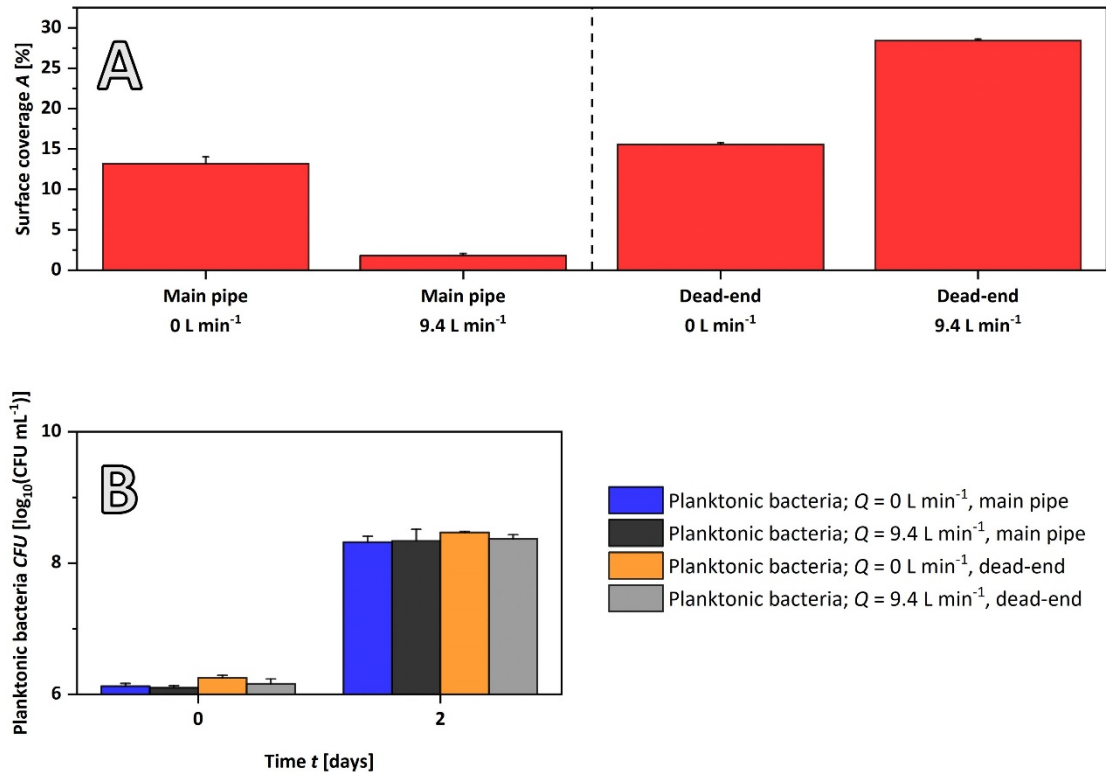


Figure 6: (A) *E. coli* biofilm surface coverage of PMMA slides after two days of growth in LB growth medium in the DWDS at different flow regimes in the main pipe. The flow cell was located either in the main pipe or in the dead-end. (B) the concentration of planktonic bacteria at the beginning and at the end of the experiment. The initial inoculum concentration was $10^6 \text{ CFU} \cdot \text{mL}^{-1}$. Mean values \pm SD are shown ($n = 2$).

4. Simulation of hydrodynamic flow in the model DWDS

The significantly increased biofilm growth in the dead-end with an established turbulent flow in the main pipe is surprising and could be due to the increased mass transfer into the dead-end. To check this the hydrodynamic conditions in the flow cell located in the dead-end as well as in the main pipe have been simulated. The results for the normalized flow velocity and shear stress for the flow cell located in the main pipe are given in Fig. 7. Upon entry in the flow cell,

the flow velocity increases. This is due to the change of geometry from round to rectangular at the inlet of the flow cell. Despite the uniform geometry in the flow cell, velocity increased along the length of the flow cell, which indicates that the hydrodynamic flow was not fully developed inside the flow cell. For instance, along the length of the biofilm, the flow velocity increased by 7.5 % at $52.0 \text{ L} \cdot \text{min}^{-1}$ volumetric flow. When the fluid exited the flow cell the flow velocity decreased again due to the change of the geometry (from rectangular to round). In a cross-section of the flow cell, a characteristic parabolic velocity profile was observed. The profile was flatter in the case of turbulent flow. The average shear forces at the wall (τ_{wall}) increased with the volumetric flow rate through the main pipe by more than three orders of magnitude from 0.07 Pa at $0.6 \text{ L} \cdot \text{min}^{-1}$ to 158.84 Pa at $52.0 \text{ L} \cdot \text{min}^{-1}$ volumetric flow. A marked decrease in the normalized shear stress at the entry into the flow cell (Fig. 7D) was a result of pressure drop.

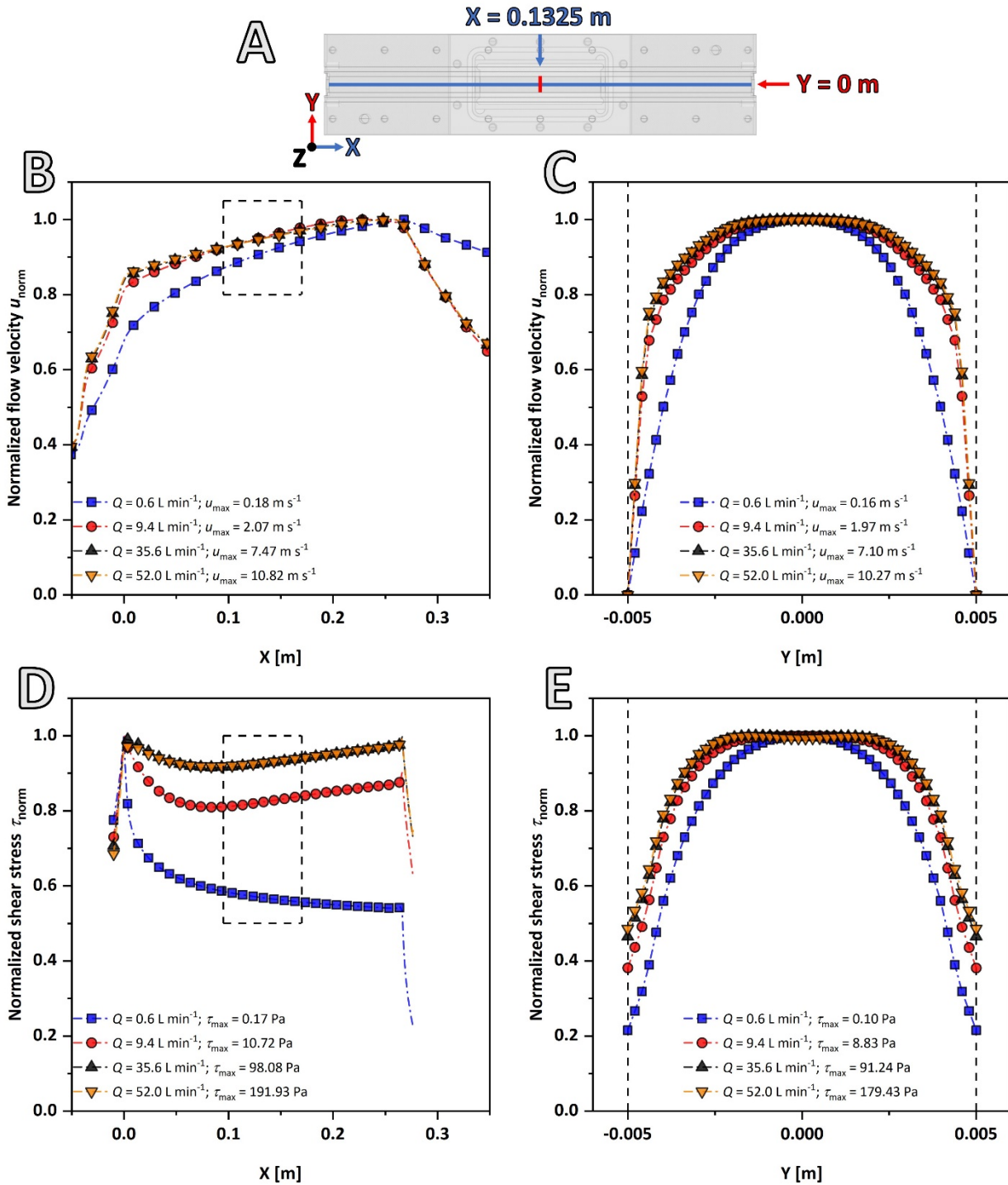


Figure 7: Schematic representation of the flow cell in the main pipe. The flow was in the X-axis direction, from left to right (A). The normalized values of the flow velocity inside the flow cell along the X direction (B) and across the flow cell in the Y direction (C), at $Z = 0$ m (middle of the pipe). The normalized values of shear stress inside the flow cell along the X direction (D) and across the flow cell in the Y direction (E), at $Z = -0.005$ m. The dashed rectangles in B, D indicate the position of the biofilm inside the flow cell. In B and D, every twentieth point is displayed for clarity.

The flow conditions in the dead-end were very different (Fig. 8). Upon entry of the flow in the dead-end, secondary flow developed and eddy formation was observed. The formation of eddies became less intense as the flow moved deeper into the dead-end. The flow velocity decreased exponentially from the entry point (Fig. 8A) to the site of biofilm growth (Fig. 8D) by more than four orders of magnitude. The fluid velocity in the dead-end was depended on the volumetric flow rate in the main pipe. Under laminar flow conditions, the flow did not ingress the dead-end pipe deeper than the entry point (Fig. 8A). As the volumetric flow rate in the main pipe increased, fluid flow entered the dead-end and eddies formed deeper in the dead-end (Fig. 8B) where the flow swirled and began to flow out of the dead-end. In the case of laminar flow, the flow velocity was $40 \text{ nm} \cdot \text{s}^{-1}$, which is very low and comparable to the diffusion of a glucose molecule over a distance of 1 cm (i.e. Péclet number, $Pe = 0.8$). On the other hand, in the case of turbulent flow in the main pipe, the flow velocity was several orders of magnitude higher (i.e. $2.6 \text{ mm} \cdot \text{s}^{-1}$ at $52.0 \text{ L} \cdot \text{min}^{-1}$, respectively). This indicates that nutrients in the dead-end can reach the flow cell with the biofilm via an advective flow. This may increase the growth rate of bacteria as observed. One should, however, be careful not to over-interpret the low velocities observed beyond the entry point in the dead-end. Flow velocities inside the flow cell further decreased (Fig. 8C) and were, at the location of biofilm (Fig. 8D), lower than $13 \text{ } \mu\text{m} \cdot \text{s}^{-1}$ even in the case of flushing turbulent conditions in the main pipe. This is apparently not sufficient to remove the biofilm.

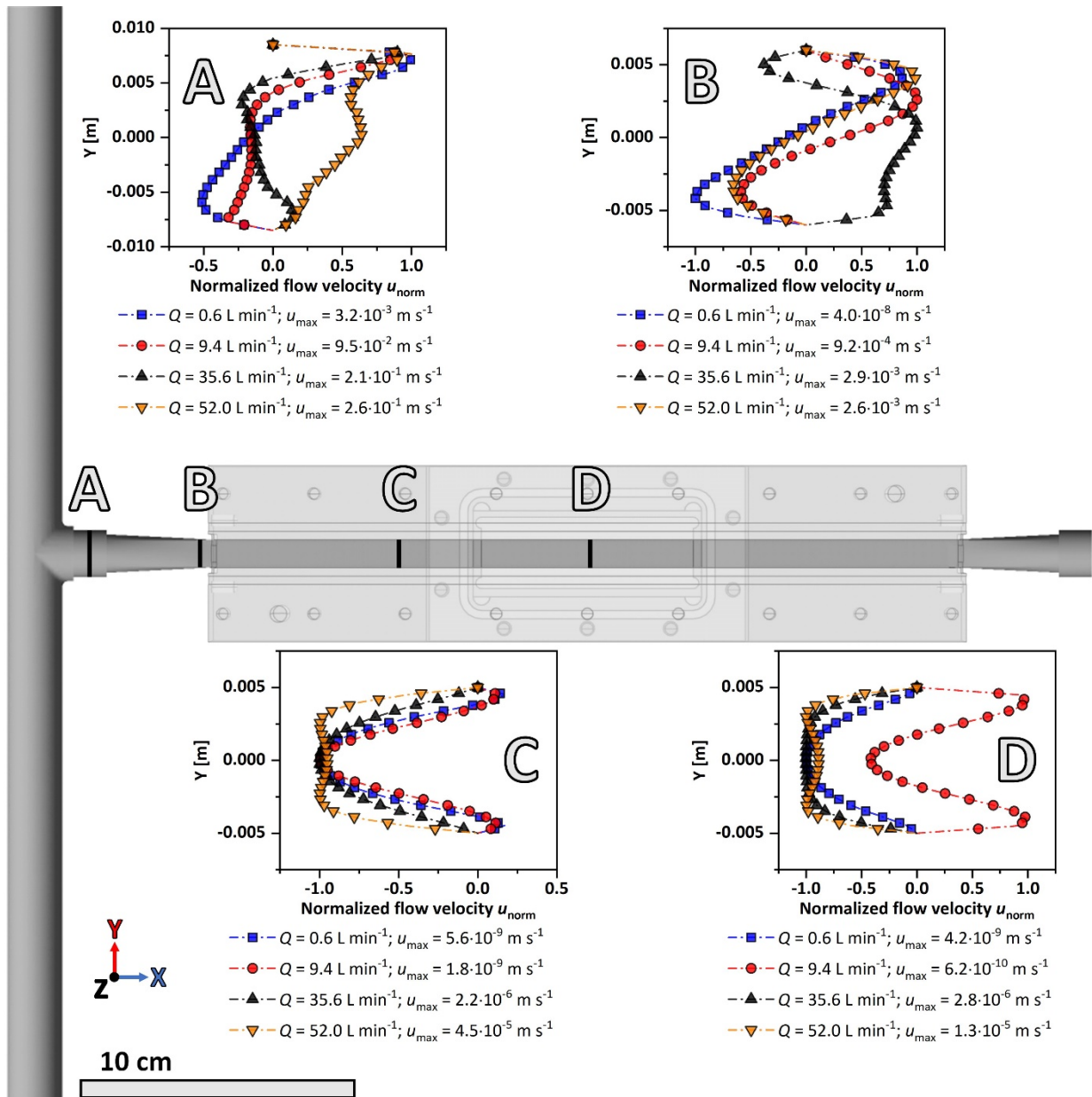


Figure 8: Velocity profiles inside the dead-end pipe as a function of the fluid volumetric flow rate in the main pipe. The graphs show the normalized flow velocity in the dead-end at different distances from the main pipe (inset figures A, B, C, and D). The transverse flow velocity profiles are shown. Negative values of flow velocity indicate a reversal of the direction of the flow. The flow inside the main pipe is along the Y-axis, from the bottom to the top. Every fifth point is displayed for clarity. Scale bar = 10 cm.

DISCUSSION

In this work, we have studied the effect of hydrodynamic forces on the growth and removal of biofilms in the main pipe and in the dead-end of a model drinking water distribution system. The results suggest that growth of the biofilm in the main pipe cannot be prevented at a volumetric flow rate of $9.4 \text{ L} \cdot \text{min}^{-1}$ and flow velocity of $2 \text{ m} \cdot \text{s}^{-1}$. Nevertheless, the surface coverage was significantly reduced compared to no shear conditions. It has been suggested that in drinking water distribution systems circulating flow velocities should not be less than $1 \text{ m} \cdot \text{s}^{-1}$ in order to prevent biofilm growth (Melo, 2003). Thomen et al., 2017 even reported that shear stress as low as 11 mPa was sufficient to prevent the initial biofilm formation. In our case, the *E. coli* biofilms formed at $2 \text{ m} \cdot \text{s}^{-1}$ and the average shear stress of 7.53 Pa. The shear force threshold for biofilm removal has been shown to fluctuate markedly (by 4 orders of magnitude) among different bacterial species and depends on the surface properties as well as the method used (Boks et al., 2008).

Increasing the volumetric flow rate in the main pipe increased biofilm removal from the surface. This is consistent with the findings of Moreira et al., 2014a; Moreira et al., 2014b; Stoodley et al., 1998. The removal of the biofilm was dependent on the biofilm maturity. Mature biofilms were more difficult to remove in our DWDS. The dependence of biofilm morphology on flow conditions has been described previously (Stoodley et al., 1998; van Loosdrecht et al., 1995). Biofilms grown in the turbulent flow regime form monolayers, which are more resilient to removal (Lapidou et al., 2005). Consistently cells farther from the wall are easier to remove by shear stress (Hwang et al., 2017; Jayathilake et al., 2017; Paul et al., 2012). Although the results suggest that more biofilm is removed with increased shear force, hydrodynamic stress alone was not sufficient to completely remove biofilms. Similar conclusions have been reached by Salta et al., 2013; Stoodley et al., 1998; and Thomen et al., 2017. Furthermore, we have

observed that if biofilms were grown in the model DWDS under shear stress conditions, they could withstand significantly higher average shear stresses (about 20 times higher) than those to which they were exposed during growth. This is consistent with the results of Hwang et al., 2014 who noticed that biofilms could not be removed by shear forces 10 times higher than those under which the biofilms grew. Lapidou and Aravas (2007) predicted that the value of Young's modulus can be influenced by the change of biofilm porosity during deformation. As a result, biofilm consolidation occurs (i.e., closing or collapsing of voids), which leads to an increase of the elastic modulus. In particular water extrusion from the biofilm makes the structure more rigid. This biofilm hardening effect was observed experimentally (Picioreanu et al., 2018). In our experiments, we have used high inoculum concentrations (10^6 CFU · mL⁻¹) and rich growth medium to probe the potential of bacteria to form biofilms under shear stress conditions. This represents a worst-case scenario for DWDS. Such conditions increase the frequency of collisions of bacteria with the surface, but should not interfere with the hydrodynamic prevention of biofilm formation. If a bacterium has the potential to adhere to the surface, it is a question of time when it will adhere and grow to a mature biofilm. In real DWDS the potential is usually realized in the course of months or years (Martiny et al., 2003), whereas in our case we have sped this up considerably. The results of this study indicate that for a complete removal of biofilms from the main pipe, Reynolds numbers above 10^5 and the average shear stress in excess of 150 Pa would be required. This is not feasible in real water distribution systems. Nevertheless, applying a high shear rate can significantly decrease biofilm-related surface coverage problems.

Much less is known about the growth and removal of biofilms in dead-ends of water distribution systems. Dead-ends may account for 25 % or more of the water distribution system volume (Tzatchkov et al., 2002). Development of biofilm in a dead-end filtration system has been

described (Kerdi et al., 2019). Biofilms had structural behavior similar to elastic material. However, a hysteresis-like trend appeared with maturation suggesting the viscoelastic nature of the biofilm. Conditions inside the dead-end are often compared to stagnant conditions (Liu et al., 2006; Smith et al., 1999; Zlatanović et al., 2017). In our model DWDS, we have observed that with increasing volumetric flow rate in the main pipe the biofilm surface coverage in the dead-end increased significantly. This suggests that mass transfer into the dead-end is possible. The flow simulations in the dead-end indicate the existence of eddy formation and secondary flow at the entrance into the dead-end. Deeper into the dead-end flow velocity decreased exponentially. This is not consistent with the generally accepted notion of stagnant conditions in the dead-end. Further support for non-stagnant conditions inside the dead-end comes from an increased biofilm growth during the turbulent flow in the main pipe, but not during the stagnant conditions in the main pipe. At the location of the biofilm (200 mm into the dead-end), the flow velocity was 9 orders of magnitude lower compared to the main pipe. At such low flow velocities comparable to the diffusion of molecules, no significant removal of biofilms can be expected. Consistently, we have observed that flushing the system with $Q = 52.0 \text{ L min}^{-1}$ had no effect on the removal of biofilm from the dead-end. The simulation results show that at the depth of one pipe diameter inside the dead-end, the flow conditions are already not sufficient to remove the biofilm. Dead-ends with lengths that are larger than one pipe diameter are frequently found in DWDS and are very problematic because bacteria can colonize them and find refuge that protects them from flushing. More worrying, the results seem to imply that bacteria grow faster in such locations due to the constant influx of nutrients and therefore represent a possible source for colonization of the rest of the water distribution system. Thick biofilms that can grow in the dead-ends are also much more resistant to chemical challenges (Costerton, 1999; Mah and O'Toole, 2001; Stewart, 2015).

CONCLUSIONS

A major challenge for the drinking water industry is to provide a microbiologically and chemically safe product with appropriate organoleptic properties. Controlling biofilm growth in water distribution systems remains one of the major challenges. The results of this study suggest that biofilm growth and removal in the main pipe system can be, to a limited extent, controlled with different flow regimes. Water flow velocities higher than $2 \text{ m} \cdot \text{s}^{-1}$ reduced bacterial adhesion significantly, but could not prevent biofilm growth. Far less effective was the control of biofilms in the dead-end. Bacteria found refuge in the dead-end and grew faster with established flow in the main pipe. The hydrodynamic flow simulation and biofilm growth experiments suggested that water in the dead-end was not stagnant. Although the flow velocity inside the dead-end decreased exponentially, it allowed increased biofilm growth at large distances from the entrance (i.e. 200 mm). Compared to stagnant conditions, biofilm grew twice as fast inside the dead-end when conditions in the main pipe were turbulent. We conclude that biofilms cannot be hydrodynamically removed from the dead-end at depths that are larger than one pipe diameter.

Acknowledgments

The authors acknowledge the financial support from the Slovenian Research Agency (research core funding No. P2-0401 and P4-0116). We would like to thank Mr. Tone Godeša for producing test rig.

References

Barbeau B., Julienne K., Carriere A., Gauthier V. 2005. Dead-end flushing of a distribution system: Short and long-term effects on water quality. *Journal of Water Supply: Research and Technology-Aqua*, 54, 6: 371–383, doi:10.2166/aqua.2005.0035

Baš S., Kramer M., Stopar D. 2017. Biofilm Surface Density Determines Biocide Effectiveness. *Frontiers in Microbiology*, 8, doi:10.3389/fmicb.2017.02443

Boks N. P., Norde W., van der Mei H. C., Busscher H. J. 2008. Forces involved in bacterial adhesion to hydrophilic and hydrophobic surfaces. *Microbiology*, 154, 10: 3122–3133, doi:10.1099/mic.0.2008/018622-0

Carter J. T., Lee Y., Buchberger S. G. 1997. Correlations between travel time and water quality in a deadend loop. *Proc. Wat.Qual. Technol. Conf. Am. Wat. Wks Assoc.*, November 9 – 12, Denver, Co, USA.

Characklis W.G. 1990. Biofilm processes. In: *Biofilms*. Characklis W.G., Marshall K.C. (eds.). New York, Wiley: 195-231

Costerton J. W. 1999. Bacterial Biofilms: A Common Cause of Persistent Infections. *Science*, 284(5418), 1318–1322. doi:10.1126/science.284.5418.1318

Douterelo I., Husband S., Loza V., Boxall J. 2016. Dynamics of Biofilm Regrowth in Drinking Water Distribution Systems. *Applied and Environmental Microbiology*, 82(14), 4155–4168, doi:10.1128/aem.00109-16

Douterelo I., Sharpe R. L., Boxall J. B. 2013. Influence of hydraulic regimes on bacterial community structure and composition in an experimental drinking water distribution system. *Water Res* 47:503–516. doi:10.1016/j.watres.2012.09.053

Elgamal M., Farouk M. 2019. Experimental Investigation of Purging Saline Solution from a Dead-End Water Pipe. *Water*, 11(5), 994. doi:10.3390/w11050994

Elger D.F., Williams B.C., Crowe C. T., Roberson J.A., *Engineering Fluid Mechanics - 10th edition*, Wiley (2012)

Ferziger J. H., Perić M., 2002. *Computational Methods for Fluid Dynamics*, Springer-Verlag Berlin, Heidelberg, New York

Herigstad B., Hamilton M., Heersink J. 2001. How to optimize the drop plate method for enumerating bacteria. *Journal of Microbiological Methods*, 44(2), 121–129. doi:10.1016/s0167-7012(00)00241-4

Horvat M., Pannuri A., Romeo T., Dogša, I., Stopar D. 2019. Viscoelastic response of *Escherichia coli* biofilms to genetically altered expression of extracellular matrix components. *Soft Matter*, 15, 25: 5042–5051, doi:10.1039/c9sm00297a

Hwang G., Klein M. I., Koo H. 2014. Analysis of the mechanical stability and surface detachment of mature *Streptococcus mutans* biofilms by applying a range of external shear forces. *Biofouling*, 30(9), 1079–1091. doi:10.1080/08927014.2014.969249

Hwang G., Liu Y., Kim D., Li Y., Krysan D. J., Koo H. 2017 *Candida albicans* mannans mediate *Streptococcus mutans* exoenzyme GtfB binding to modulate cross-kingdom biofilm development in vivo. *PloS Pathogens*, 13, 6: e1006407, <https://doi.org/10.1371/journal.ppat.1006407>

Jayathilake P. G., Gupta P., Li B., Madsen C., Oyebamiji O., González-Cabaleiro R., Rushton S., Bridgens B., Swailes D., Allen B., McGough A. S., Zuliani P., Ofiteru D. I., Wilkinson D.,

Chen J., Curtis T. 2017. A mechanistic Individual-based Model of microbial communities. *PLoS ONE*, 12, 8: e0181965, doi:10.1371/journal.pone.0181965

Kerdi S., Qamar A., Alpatova A., Ghaffour N., An in-situ technique for the direct structural characterization of biofouling in membrane filtration. 2019. *Journal of Membrane Science* 583: 81-92, doi.org/10.1016/j.memsci.2019.04.051

Lapidou C.S., Rittmann B.E., Karamanos S.A. 2005. Finite element modeling to expand the UMCCA model to describe biofilm mechanical behavior. *Water Science & Technology*, 52, 7: 161-166, doi.org/10.2166/wst.2005.0196

Lapidou C. S., Aravas N., 2007. Variation in mechanical properties of a porous multi-phase biofilm under compression due to void closure. *Water Science & Technology*, 55(8-9): 447-53

LeChevallier M. W. 2003. Conditions favouring coliform and HPC bacterial growth in drinking-water and on water contact surfaces. In: *Heterotrophic Plate Count Measurement in Drinking Water Safety Management*. Bartram J., Cotruvo J., Exner M., Fricker C., Glasmacher A. (eds.). Geneva, World Health Organization, 177-198

Ling F., Whitaker R., LeChevallier M. W., Liu, W.-T. 2018. Drinking water microbiome assembly induced by water stagnation. *The ISME Journal*, 12(6), 1520–1531. doi:10.1038/s41396-018-0101-5

Liu N., Skauge T., Landa-Marbán D., Hovland B., Thorbjørnsen B., Radu F. A., Vik B. F., Baumann T., Bødtker G. 2019. Microfluidic study of effects of flow velocity and nutrient concentration on biofilm accumulation and adhesive strength in the flowing and no-flowing microchannels. *Journal of Industrial Microbiology & Biotechnology*, 46: 6, doi:10.1007/s10295-019-02161-x

Liu S., Gunawan C., Barraud N., Rice S. A., Harry E. J., Amal R. 2016. Understanding, Monitoring, and Controlling Biofilm Growth in Drinking Water Distribution Systems. *Environmental Science & Technology*, 50, 17: 8954–8976, doi:10.1021/acs.est.6b00835

Liu Z., Lin Y. E., Stout J. E., Hwang C. C., Vidic R. D., Yu V. L. 2006. Effect of flow regimes on the presence of *Legionella* within the biofilm of a model plumbing system. *Journal of Applied Microbiology*, 101, 2: 437–442, doi:10.1111/j.1365-2672.2006.02970.x

Lorenzetti M., Dogša I., Stošicki T., Stopar D., Kalin M., Kobe S., Novak S. 2015. The Influence of Surface Modification on Bacterial Adhesion to Titanium-Based Substrates. *ACS Applied Materials & Interfaces*, 7, 3: 1644–1651, doi:10.1021/am507148n

Mah T.-F. C., O’Toole G. A. 2001. Mechanisms of biofilm resistance to antimicrobial agents. *Trends in Microbiology*, 9(1), 34–39. doi:10.1016/s0966-842x(00)01913-2

Martiny A. C., Jorgensen T. M., Albrechtsen H.-J., Arvin E., Molin S. 2003. Long-Term Succession of Structure and Diversity of a Biofilm Formed in a Model Drinking Water Distribution System. *Applied and Environmental Microbiology*, 69(11), 6899–6907. doi:10.1128/aem.69.11.6899-6907.2003

McVay R.D. Effective Flushing Techniques for Water Systems. Florida Rural Water Association. Available online: <http://www.frwa.net/uploads/4/2/3/5/42359811/effectiveflushingtechniquesforwatersystems051608.doc> (accessed on 9 April 2019).

Melo F. L. 2003. Biofilm formation and its role in fixed film processes. *Handbook of Water and Wastewater Microbiology*, 337–349. doi:10.1016/b978-012470100-7/50021-2

Menter F. R. 1994. Two-equation eddy-viscosity turbulence models for engineering applications. *AIAA Journal*, 32(8), 1598–1605. doi:10.2514/3.12149

Moreira J. M. R., Araújo J. D. P., Miranda J. M., Simões M., Melo L. F., Mergulhão F. J. 2014. The effects of surface properties on *Escherichia coli* adhesion are modulated by shear stress. *Colloids and Surfaces B: Biointerfaces*, 123: 1–7, doi:10.1016/j.colsurfb.2014.08.016

Moreira J. M. R., Simões M., Melo L. F., Mergulhão F. J. 2014. The combined effects of shear stress and mass transfer on the balance between biofilm and suspended cell dynamics. *Desalination and Water Treatment*, 53, 12: 3348–3354, doi:10.1080/19443994.2014.933625

Paul E., Ochoa J. C., Pechaud Y., Liu Y., Liné A. 2012. Effect of shear stress and growth conditions on detachment and physical properties of biofilms. *Water Research*, 46, 17: 5499–5508, doi:10.1016/j.watres.2012.07.029

Patankar S.V. 1980. *Numerical heat transfer and fluid flow*, 1st ed. Hemisphere Publishing Corporation, New York

Piciooreanu C., Blauert F., Horn H., Wagner M., 2018. Determination of mechanical properties of biofilms by modelling the deformation measured using optical coherence tomography. *Water Research*, 145, 15: 588-598, doi.org/10.1016/j.watres.2018.08.070

Salta M., Capretto L., Carugo D., Wharton J. A., Stokes K. R. 2013. Life under flow: A novel microfluidic device for the assessment of anti-biofilm technologies. *Biomicrofluidics*, 7, 6: 064118, doi:10.1063/1.4850796

Simões L. C., Simões M. 2013. Biofilms in drinking water: problems and solutions. *RSC Advances*, 3, 8: 2520–2533, doi:10.1039/c2ra22243d

Smith S. E., Holt D. M., Delanoue A., Colbourne J. S., Chamberlain A. H. L., Lloyd B. J. 1999. A pipeline testing facility for the examination of pipe wall deposits and red-water events in drinking water. *Journal of the Chartered Institution of Water and Environmental Management*, 1, 13: 7–15.

Soini S., Koskinen K., Vilenius M., Puhakka J. 2002. Effects of fluid-flow velocity and water quality on planktonic and sessile microbial growth in water hydraulic system. *Water Research*, 36(15), 3812–3820. doi:10.1016/s0043-1354(02)00099-4

Sommerfeld M., Huber N. 1999. Experimental analysis and modelling of particle-wall collisions. *International Journal of Multiphase Flow*, 25(6-7), 1457–1489. doi:10.1016/s0301-9322(99)00047-6

Stewart P. S. 2015. Antimicrobial Tolerance in Biofilms. *Microbiology Spectrum*, 3(3). doi:10.1128/microbiolspec.mb-0010-2014

Stoodley P., Cargo R., Rupp C. J., Wilson S., Klapper I. 2002. Biofilm material properties as related to shear-induced deformation and detachment phenomena. *Journal of Industrial Microbiology and Biotechnology*, 29, 6: 361–367, doi:10.1038/sj.jim.7000282

Stoodley P., Dodds I., Boyle J. D., Lappin-Scott H. M. 1998. Influence of hydrodynamics and nutrients on biofilm structure. *Journal of Applied Microbiology*, 85, S1: 19S–28S, doi:10.1111/j.1365-2672.1998.tb05279.x

Teodósio J. S., Silva F. C., Moreira J. M. R., Simões M., Melo L. F., Alves M. A., Mergulhão F. J. 2013. Flow cells as quasi-ideal systems for biofouling simulation of industrial piping systems. *Biofouling*, 29, 8: 953–966, doi:10.1080/08927014.2013.821467

Teodósio J. S., Simões M., Alves M. A., Melo L. F., Mergulhão F. J. 2012. Setup and Validation of Flow Cell Systems for Biofouling Simulation in Industrial Settings. *The Scientific World Journal*, 2012, 8: 1–10, doi:10.1100/2012/361496

Thomen P., Robert J., Monmeyran A., Bitbol A.-F., Douarche C., Henry N. 2017. Bacterial biofilm under flow: First a physical struggle to stay, then a matter of breathing. *PLoS ONE*, 12, 4: e0175197, doi:10.1371/journal.pone.0175197

Tosun I., Uner D., Ozgen C., Critical Reynolds number for Newtonian flow in rectangular ducts, *Industrial & Engineering Chemistry Research*, 1988, 27(10)

Tzatchkov V. G., Aldama A. A., Arreguin F. I. 2002. Advection-Dispersion-Reaction Modeling in Water Distribution Networks. *Journal of Water Resources Planning and Management*, 128, 5: 334–342, doi:10.1061/(asce)0733-9496(2002)128:5(334)

van Loosdrecht M. C. M., Eikelboom D., Gjaltema A., Mulder A., Tjihuis L., Heijnen, J. J. 1995. Biofilm structures. *Water Science and Technology*, 32, 8: 35-43, doi:10.1016/0273-1223(96)00005-4

Zack G. W., Rogers W. E. Latt S. A. 1977. Automatic measurement of sister chromatid exchange frequency. *Journal of Histochemistry & Cytochemistry*, 25(7), 741–753. doi:10.1177/25.7.70454

Zlatanović L., van der Hoek J. P., Vreeburg J. H. G. 2017. An experimental study on the influence of water stagnation and temperature change on water quality in a full-scale domestic drinking water system. *Water Research*, 123: 761–772. doi:10.1016/j.watres.2017.07.019